Application of European CFD Methods for Helicopter Rotors in Forward Flight[1]

M. Costes*, R. Houwink**, A. Kokkalis+, K. Pahlke++, A. Saporiti+++

* ONERA, Châtillon, France

** NLR, Amsterdam, The Netherlands

+ WHL, Yeovil, U.K.

++ DLR, Braunschweig, Germany

+++ Agusta, Cascina Costa Di Samarate, Italy

Abstract

This paper presents development and validation of European CFD codes for helicopter rotors. This work was completed during the BRITE/EURAM DACRO project. The methods were compared on test cases selected in common, dealing with rotors in high speed forward flight. The methods tested cover a wide range of formulations available to compute such a complex flow, from 2D unsteady viscous TSP, 2D unsteady Euler, to 3D quasi-steady and unsteady potential, with or without boundary layer corrections. The results show that the flow unsteadiness and three-dimensionality are important to describe the transonic zone correctly.

1 Introduction

In the helicopter industry, the development and use of CFD is less advanced than for fixed wing aircraft, mainly because of the complexity of helicopter rotors (articulated blade, unsteady flow, transonic advancing blade, retreating blade stall...). Naturally, the progress made in CFD for fixed wing is used in rotorcraft, but further development is necessary because of rotor flow unsteadiness and complexity.

Within the BRITE/EURAM programme DACRO, several European CFD codes for rotors were improved and validated on common test cases [1]. The purpose of this paper is to present a synthesis of the computations performed for high-speed forward flight. The different methods used are a two-dimensional transonic small perturbations code including viscous effects with a strong coupling technique, a two-dimensional unsteady Euler code, a three-dimensional quasi-steady transonic small perturbations code, a three-dimensional non-conservative full potential code, in unsteady or quasi-steady formulation, and an unsteady conservative full-potential code (with or without boundary layer corrections, given by an unsteady three-dimensional turbulent boundary layer code in integral form). The configurations calculated were isolated rotor test cases obtained in the ONERA S2Ch wind-tunnel. The test cases selected concern two nonlifting rotors at high-speed forward flight, one with a straight tip and the other with a swept tip, and a lifting rotor equipped with rectangular blades, also in high-speed forward flight.

1 This work was supported by the EEC through the BRITE/EURAM DACRO programme

A comparison of the various methods shows the level of agreement which can be obtained with experiment for increasing levels of sophistication. In particular, the importance of flow three-dimensionality, unsteadiness, viscosity, potential assumption and small disturbances hypothesis can be discussed. Furthermore, by integrating the computed pressure distribution, the lift values are compared to the results given by a standard industry rotor code and to experiment, thus widening the interest of the comparison.

2 Computational methods

2.1 2D unsteady methods

At DLR, an existing 2D Euler solver was used to develop an unsteady version, capable of computing the flow on a rotor blade section [2]. The method is discretized using a cell centered finite volume formulation for the relative velocity, in a rigid grid fixed to the airfoil. This central numerical scheme is second order accurate in the regions where the grid is sufficiently smooth and is stabilized by explicit artificial viscosity, using second and fourth order dissipations incorporated with adaptive coefficients. A tangency condition (vanishing normal flux) is imposed on the airfoil surface. In the far field, nonreflecting boundary conditions using either Riemann invariants or characteristics variables, are used. The time dependent equation is solved with an explicit Runge-Kutta multi-stage time stepping scheme, with a simplified evaluation of the dissipative flux terms. Speed-up techniques, such as implicit residual smoothing, are implemented in order to improve the code efficiency.

At NLR, an existing unsteady TSP code with strong viscous effects was modified to include the effect of a variable free-stream Mach number [3]. The equations are solved in a coordinate system rotating with the blade. The inviscid TSP solver computes the development of the flow with time on a rectangular grid using an ADI method for each time step. The viscous calculation is a modified version of Green's lag-entrainment method for the turbulent boundary layer and the wake. The initial laminar part of the boundary layer is computed using the compressible version of the method of Thwaites. A strong coupling between the viscous and the inviscid zones is ensured by simultaneously solving the z-sweep of the ADI method, in which boundary conditions on the airfoil are implemented, along with the boundary layer equations. This allows the efficient computation of attached as well as separated flow.

2.2 3D methods

At ONERA, an unsteady 3D conservative full potential code, FP3D, was improved and validated [4]. It solves the mass-conservation and the Bernoulli equations in a blade fixed frame, using an implicit finite-difference algorithm in a generalized coordinates system. The scheme is first order in time and second order in space. A monotone, entropy satisfying, Engquist-Osher flux biasing scheme was implemented to maintain stability in the supersonic regions, thus lowering spatial accuracy to first order in the supersonic zone. The equation is solved with an approximate factorisation technique. On the blade surface, a tangency or transpiration condition, necessary to simulate the inflow, is imposed. At the grid boundaries, nonreflecting boundary conditions, derived from a linearisation of the potential equation with wave-like inputs, are applied. Viscous corrections, given by an unsteady 3D turbulent boundary layer code written in integral form, were introduced with a simple transpiration velocity technique. They explicitly modify the boundary conditions on the blade surface to simulate the boundary layer displacement effect. Since the boundary layer cannot compute separated flows, only a weak coupling between the inviscid and the viscous regions is necessary. In the present paper, only inviscid calculations are shown with this method.

At WHL, an existing 3D quasi-steady finite difference TSP algorithm (developed at DRA Farnborough) was used to compute helicopter rotor flows [5]. It is able to solve the flow over a helicopter rotor blade at arbitrary azimuth in hover or forward flight. Conventional TSP approximations are used in developing the equation, with an ordering scheme to simplify the final equation to be solved. The basic equation includes the spanwise flow terms, which are essential to the modelling of blade azimuthes away from the advancing blade, but excludes any time dependent terms. In order to ensure stability in local regions where the flow is supersonic, it is necessary to switch from central to upwind finite difference forms in a direction corresponding to the local velocity vector. The discretised algebraic system is solved using a Gauss-Seidel method and a locally adjusted relaxation scheme.

At Agusta, the 3D steady non conservative full potential code was extended to unsteady flow conditions, by adding the time dependent terms in the equation [6]. A finite difference algorithm, written in a blade fixed frame was implemented. Spatial derivatives are expressed as second order centered finite differences. The method uses Jameson rotated difference scheme to introduce implicit artificial viscosity in the supersonic region by upwinding the streamwise derivative of the flux component. Therefore the scheme is only first order for supersonic flows. An implicit ADI technique is used to solve the second order accurate centered time dependent operator. Finally, nonreflecting boundary conditions, based on a plane wave assumption, are applied at the grid boundaries.

3 Test cases

3.1 Nonlifting rotor

This nonlifting two-bladed rotor was tested in the ONERA S2Ch wind tunnel. It has a small aspect ratio, slightly tapered planform, and is equipped with symmetric NACA00XX airfoils (figure 1). Three blade sections, at 85, 90 and 95% of the rotor radius, were equipped with unsteady pressure transducers, and global performance measurements were also performed. The model was tested at high-speed forward flight (μ=0.4, 0.45, 0.5) for a rotating tip Mach number $M_{\omega R}$=0.625, corresponding to highly transonic flows on the advancing blade side.

3.2 Lifting rotor

This rotor, shown in figure 2, was also tested in the ONERA S2Ch wind tunnel. It has a rectangular planform, and is equipped with SA131XX airfoils. As for the nonlifting rotor above, the blade has a small aspect ratio and is very rigid. Again, the sections at 85, 90 and 95% of the rotor radius were instrumented with unsteady pressure transducers. The test case selected to validate the methods is a high speed forward flight case, with an advance ratio μ=0.43, a rotating tip Mach number $M_{\omega R}$=0.63, and a lift coefficient C_L/σ=0.065.

4 3D forward flight calculations

4.1 Nonlifting calculations

In this section, nonlifting calculations for rotors at high speed forward flight are presented. All the methods described above were used in the present comparison (NLR 2D

unsteady transonic small perturbation code, DLR 2D unsteady Euler solver, Westland 3D quasi-steady transonic small perturbations code, Agusta 3D non conservative unsteady full potential code and ONERA 3D conservative unsteady full potential code). This correlation then covers a wide range of theories, with the exception of 3D Euler and Navier Stokes solvers which are not currently operational for these complex flows.

Figure 3 shows the chordwise pressure evolution at r/R=0.90 and the lowest advance ratio, 0.4. The 2D methods, NLR and DLR, overpredict the shock intensity, indicating that the flow three-dimensionality strongly reduces the shock strength. The DLR Euler shock is the strongest, because viscous effects also reduce the isentropic NLR-TSP shock intensity, which is closer to the experiment and to the three-dimensional calculations. As far as three-dimensional methods are concerned, the quasi-steady Westland TSP calculation clearly underpredicts the transonic flow after ψ=90°. This is due to the absence of unsteady effects in the formulation, which are known to delay the occurrence of transonic flows. The unsteady full potential methods give the better correlation with experiment. Among them, the Agusta method gives lower transonic flows because the formulation is non conservative, and the best simulation is given by FP3D, which is very close to experiment.

Figure 4 shows the azimuthal pressure evolution at r/R=0.90 and several chordwise stations (x/c = 0.2, 0.3, 0.4 and 0.5). This representation gives a view of the transonic flow development on the blade. The 2D methods obviously overpredict the supersonic extend. Among the 3D methods, the Westland code is not time accurate with its quasi-steady hypothesis, and the shock motion is not correctly captured by the calculation. This shock motion is better predicted by the Agusta code, but it is still not quite accurate because of the non-conservative formulation. The FP3D predictions are in good agreement with experiment, and the shock excursions at each chordwise station are well predicted.

Similar calculations are shown in figures 5 and 6 for the higher advance ratio μ=0.5. Correspondingly, the shock intensity is higher, and the computer codes predict this fact correctly (figure 5). However, this very high speed case is too severe for the 2D calculations. The shock computed by the DLR Euler code is much too strong. Furthermore, the NLR code computes a fully separated flow behind the shock, which is not realistic for a real 3D configuration under these flight conditions. This shows the limit of the 2D assumption on a rotor blade. Concerning the 3D calculations, the quasi-steady Westland calculations show the same discrepancies as those seen at the lower speed, with a clear underestimation of the shock intensity at ψ=150°. The Agusta full potential code gives good results at ψ=60°, but the shock intensity is underestimated for the remaining azimuthes shown. Opposite results are found for the ONERA FP3D code, which gives reasonably good results except at ψ=60° where the shock intensity is too strong. However, the shock intensity is always slightly overestimated. At this very high speed case, the isentropic assumption may be more irrelevant, inducing then errors in the computed shock. However, the correlation is still satisfactory.

Figure 6 shows the azimuthal pressure evolution, still at the same blade section. The comments made above at μ=0.4 can be repeated. The best time accuracy is given by FP3D which computes the shock motion correctly, while the Agusta and the Westland calculations underestimate the transonic azimuthal extension, especially for the quasi-steady Westland calculations. As far as 2D methods are concerned, the comparison is less penalizing for the stations shown on the figure because, at this very high speed case, the shock excursion is greater.

4.2 Lifting calculations

The lifting configuration has been computed with the Westland TSP and the ONERA FP3D codes for the 3D methods, and by the NLR TSP and the DLR Euler codes for the 2D methods. The flight conditions are μ=0.43 and C_L/σ=0.066. For a lifting rotor, since the present CFD methods only compute an isolated blade, the blade inflow must be given by an

external model. For the present calculations, the same inflow was used for both 3D and 2D calculations. This was given by a lifting line model with fixed wake geometry (METAR code from Eurocopter France, [7]), in which the experimental blade movement (pitch, flap) was used as input. In the 3D potential methods, the near wake is taken into account in the computational domain through a branch-cut. Therefore its influence was removed from the whole METAR wake when computing the rotor inflow. In calculating the inflow angle from the METAR wake for input into the 2D unsteady codes, the effects due to both the steady and unsteady near wake were included. The unsteady 2D methods, however, also compute the unsteady contribution of the near wake. Thus in order to avoid a "double accounting" of the near wake unsteady effects, these should be removed from the calculations. This was not possible in the present research programme and thus some "double accounting" of the near wake unsteady effects is included in the present 2D calculations.

Figure 7 shows a comparison of the computed pressure distribution with experiment at r/R=0.90 for the 3D codes. The quasi-steady Westland TSP calculation was only performed on the advancing blade side, while the ONERA FP3D code computed the whole rotor revolution. The FP3D code gives good agreement with experiment for the advancing blade side, and the shock position and intensity is well computed on the upper surface, contrary to the Westland TSP calculation which, because of the quasi-steady assumption, overestimates the shock intensity before ψ=90° and underestimates this intensity after ψ=90°. On the lower surface, FP3D computes correctly the velocity peak at the leading edge, where supersonic flow is found at ψ=60° and ψ=90°, as also given by the experiment. Probably because of the small perturbation hypothesis, the TSP code does not compute this velocity peak, and large differences with experiment are found in this region. The same comparison is shown in figure 8 for the 2D methods, NLR and DLR. Reasonably good agreement is also found with experiment, but as expected, the computed shock is too strong because three-dimensional effects reduce its intensity. On the lower surface, the leading edge velocity peak is computed by both methods, but it is smaller than for the experiment or the FP3D calculations. An insufficient grid density in this region can be suspected, at least for the DLR Euler calculations. Figure 9 shows the unsteady computations for the retreating side given by the unsteady methods (3D ONERA FP3D, 2D NLR TSP and 2D DLR Euler). All the methods give very similar results and correlate well with experiment. The flow acceleration on the upper surface and the compression on the lower surface are lower in the FP3D computations, which is due to three-dimensional effects.

Figure 10 shows a comparison of the lift coefficient evolution versus the azimuth, as computed by the ONERA FP3D, the Westland TSP, the NLR TSP, the DLR Euler, the lifting line code METAR (which was used to compute the inflow as input in the CFD methods) and experiment, for two sections (85 and 90%). The lift prediction is reasonably good for all the unsteady methods on this very rigid blade, except at the azimuth ψ=0°, where interactions with the rotor hub induce a sudden lift loss in the experiment. The 2D methods tend to overestimate the section lift. On the advancing blade side, this is due to the too strong shocks found in the 2D calculations. On the retreating side of the rotor disk, the lift computed by the NLR TSP method is lower than the DLR Euler lift, which is due to viscosity included in the NLR calculations, and these viscous calculations are closer to experiment. The best correlations with experiment are given by METAR and FP3D, which give very similar results, even if they slightly underestimate the lift around ψ=180°. Westland calculations show the larger discrepancies with respect to experiment, probably because of the quasi-steady assumption. A similar comparison is shown in figure 11 for the moment coefficient. Due to its small values, conclusions are more difficult to draw. 3D methods always give a positive moment coefficient and low variations with the azimuth, this last point being in closer agreement with experiment. The 2D methods seem to give better results at r/R=0.85 and FP3D is closer to experiment at r/R=0.90. The METAR and Westland Cm values have the lower fluctuations, with METAR giving a reasonably good average value.

5 Conclusions

This limited comparison of various European CFD codes used to compute a helicopter rotor in forward flight led to the following conclusions :

– the 2D methods, viscous or inviscid, give the general behaviour of the flow occurring on a helicopter rotor blade; nevertheless, at high speed, they cannot give an accurate description of the flow, because the flow three–dimensionality has a strong influence on the shock wave's intensity, which is then overestimated by such calculations; however, as a first approach, they can be viewed as satisfactory;

– among the 3D methods tested, all of which are based upon the potential flow assumption, it was found that the TSP quasi–steady formulation is not appropriate to simulate helicopter blade flow in forward flight and for azimuth positions other than $\psi \equiv 90°$, because unsteady effects are important when shock waves or large incidence and incidence gradients occur; similarly, the small perturbation hypothesis is not satisfactory because modern helicopter airfoils have a high leading edge curvature on the lower surface; at least an unsteady full potential approach is therefore necessary; comparisons between the Agusta and the ONERA codes show that the formulation must be fully conservative to minimize errors, especially as far as shock motion and intensity is concerned; the FP3D code is seen to give the best correlations with experiment for the configurations tested, which suggests that the main flow features are included in the model; more sophisticated models, such as unsteady Euler or Navier–Stokes would probably slightly improve the correlation for the part of the rotor disk considered (outer part), but their main interest would be in their ability to capture the rotor wake and, for Navier–Stokes solvers only, for the computation of areas of rotor flow when strong viscous effects are dominant (eg shock–induced separation, dynamic stall); their computer cost, however, will be much higher than for potential models; an intermediate and efficient solution could be a strong coupling between an unsteady full potential model and the boundary layer equations.

References

[1] Various authors. Current European Rotorcraft Research Activities on Development of Advanced CFD Methods for the Design of Rotor Blades (BRITE/EURAM DACRO Project). *17th European Rotorcraft Forum*. 24–27 September 1991. Berlin, Germany.

[2] K. Pahlke. Development of a Numerical Method Solving the Unsteady Euler Equations for Airfoils in Arbitrary Motion. *DLR Report IB 129–92/09*. May 1992.

[3] R. Houwink. Computations of Unsteady Viscous Flow about Sections of Helicopter Rotor Blades in Forward Flight–Contribution to BRITE/EURAM Project DACRO, Task 4, Part 2 . *NLR CR 92196 L*. 1992.

[4] M. Costes, M. Rahaingomanana, A. Desopper. Weak Coupling Between an Unsteady 3D Full Potential Code and an Unsteady Turbulent Boundary Layer Code–Application to a Helicopter Rotor in Forward Flight. *30th AIAA Aerospace Sciences Meeting*. January 1992. Reno, Nevada.

[5] J. Grant. The Prediction of Supercritical Pressure Distributions on Blade Tips of Arbitrary Shape over a Range of Advancing Blade Azimuth Angles. *Vertica, Vol.3, pp. 275–292.* 1979.

[6] A Saporiti. Extension of a 3D Steady Full Potential Code to the Unsteady Flow Conditions. *BRITE/EURAM DACRO Report.* June 1991.

[7] W. G. Bousman, C. Young, N. Gilbert, F. Toulmay, W. Johnson, M. J. Riley. Correlation of Puma Airloads–Lifting Line and Wake Calculation. *15th European Rotorcraft Forum.* 12–15 September 1989. Amsterdam, The Netherlands.

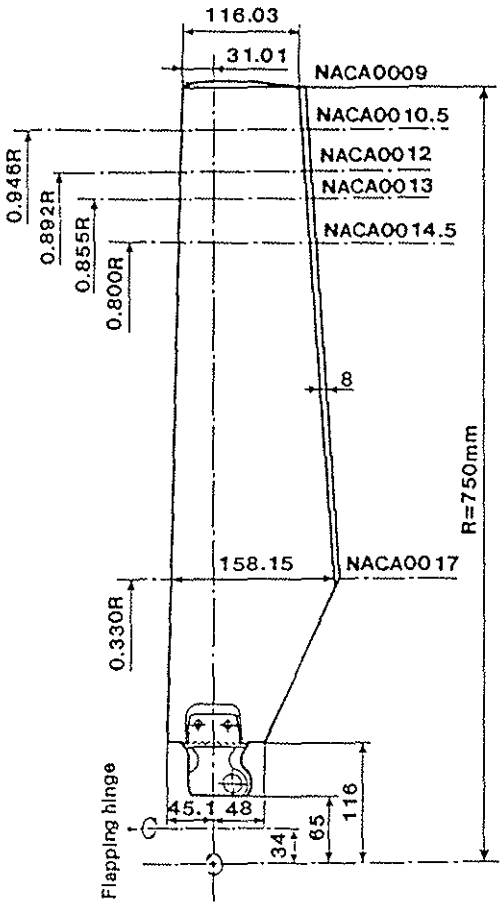

Fig. 1 - Non-lifting rotor.

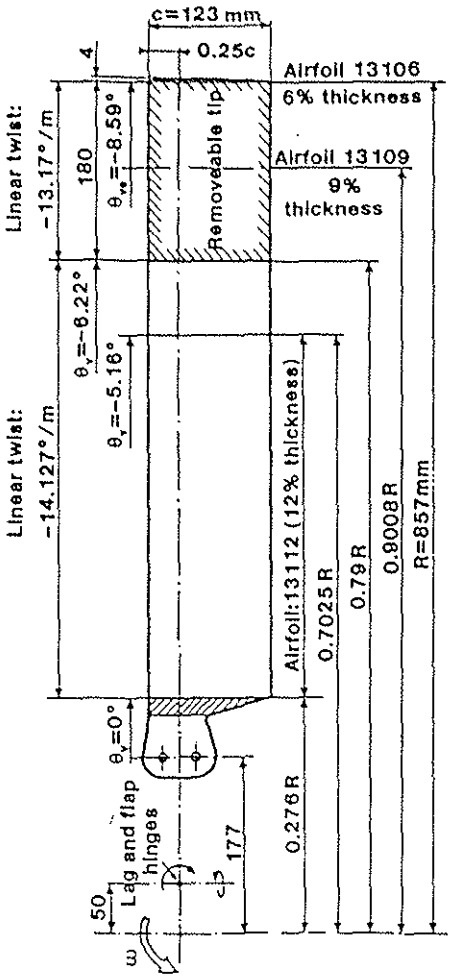

Fig. 2 - Lifting rotor

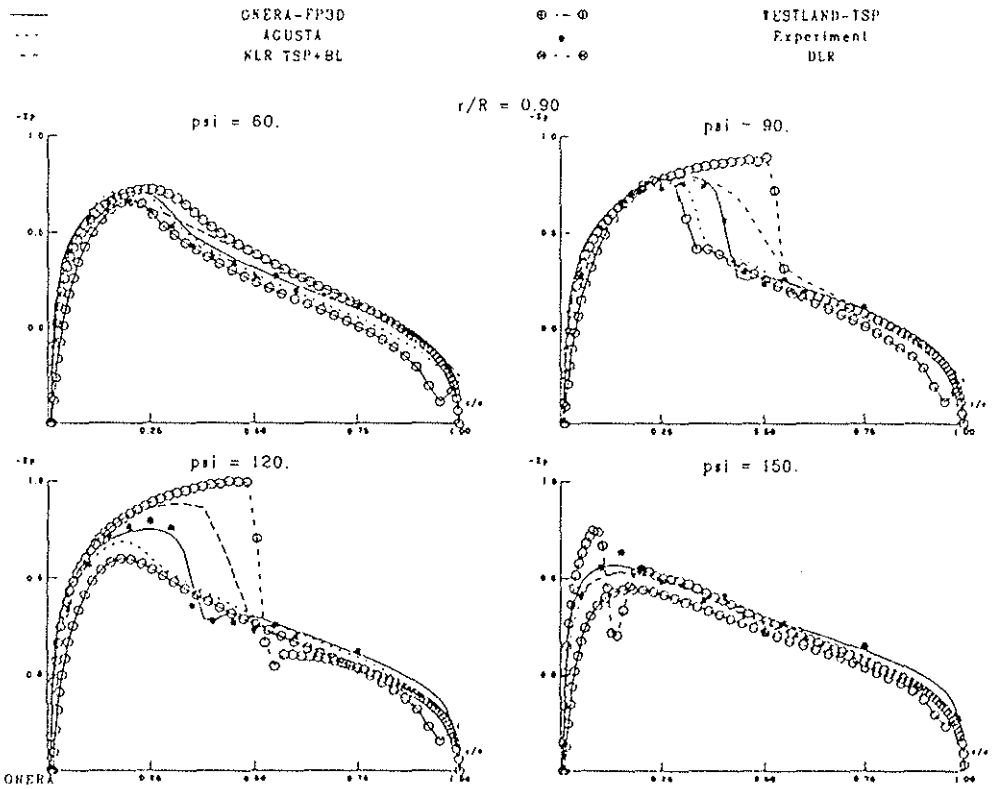

Fig. 3 - Non-lifting forward flight, $\mu = 0.40$, $M_{\omega R} = 0.625$.

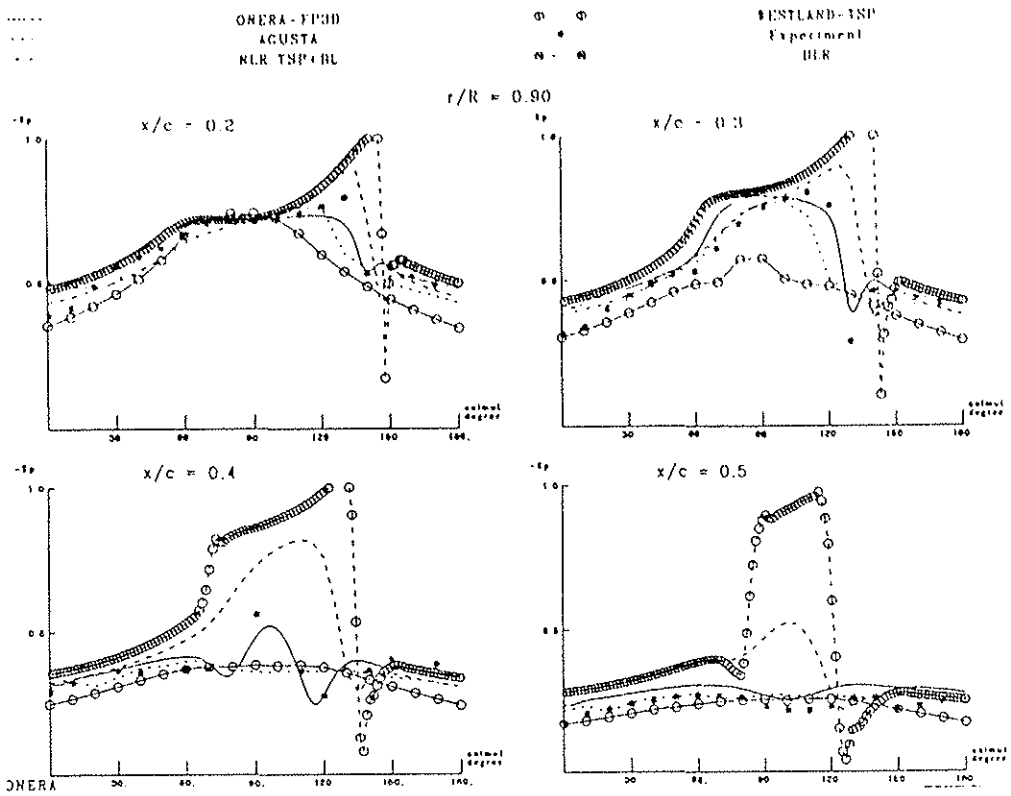

Fig. 4 - Non-lifting forward flight, $\mu = 0.40$, $M_{wR} = 0.625$.

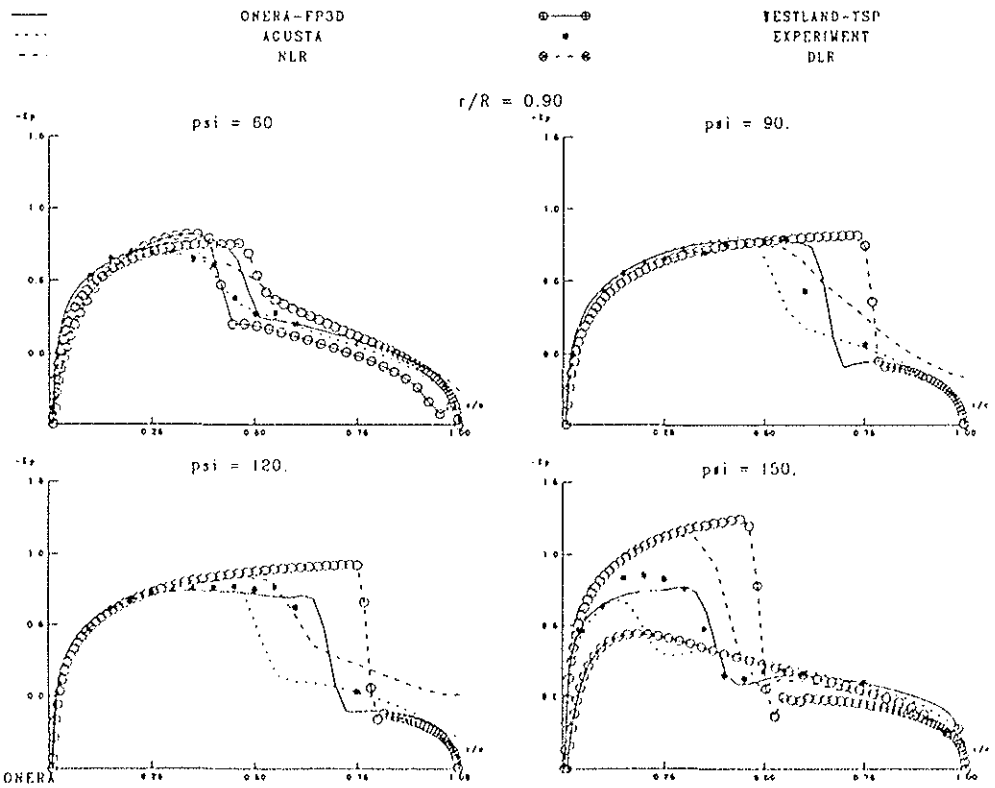

Fig. 5 - Non-lifting forward flight, $\mu = 0.50$, $M_{wR} = 0.625$.

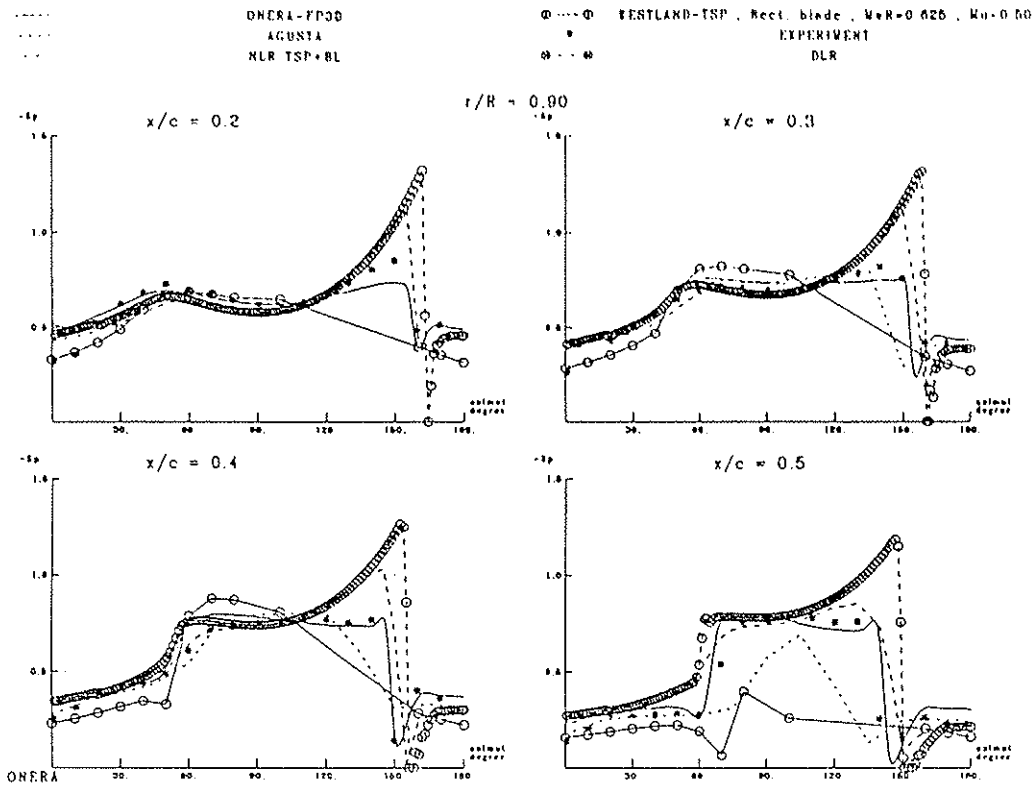

Fig. 6 - Non-lifting forward flight, $\mu = 0.50$, $M_{wR} = 0.625$.

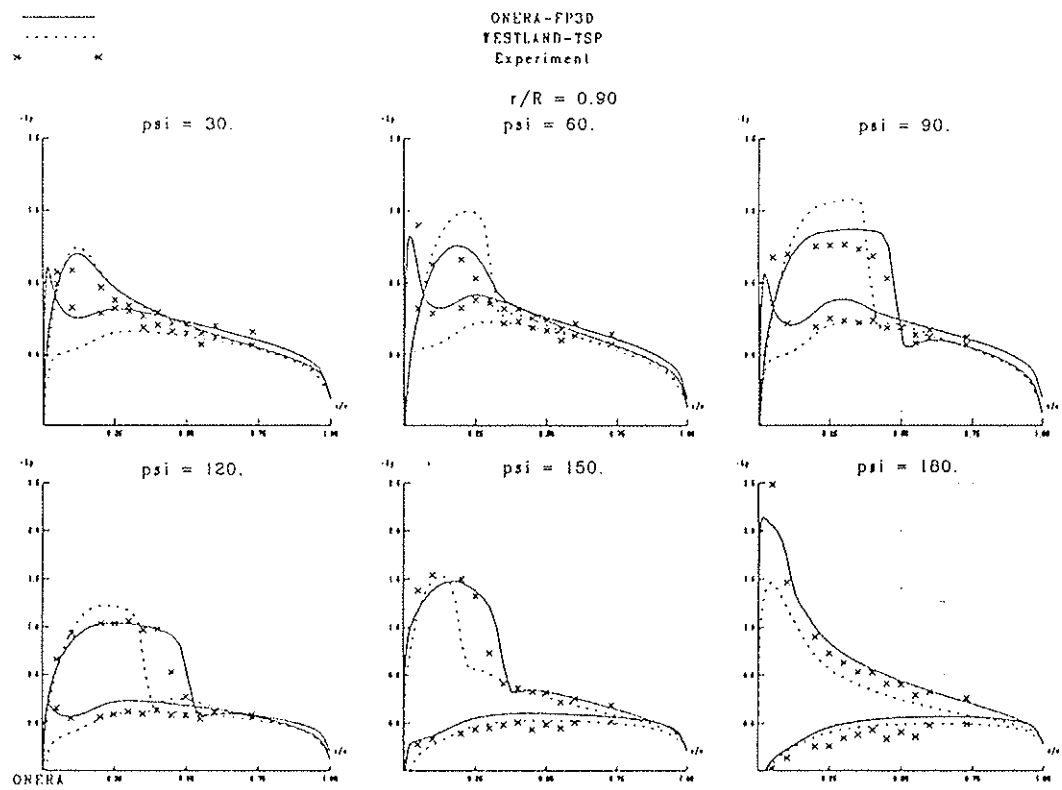

Fig. 7 - Lifting forward flight
$\mu = 0.43$, $M_{wR} = 0.63$, $C_L/\sigma = 0.066$.

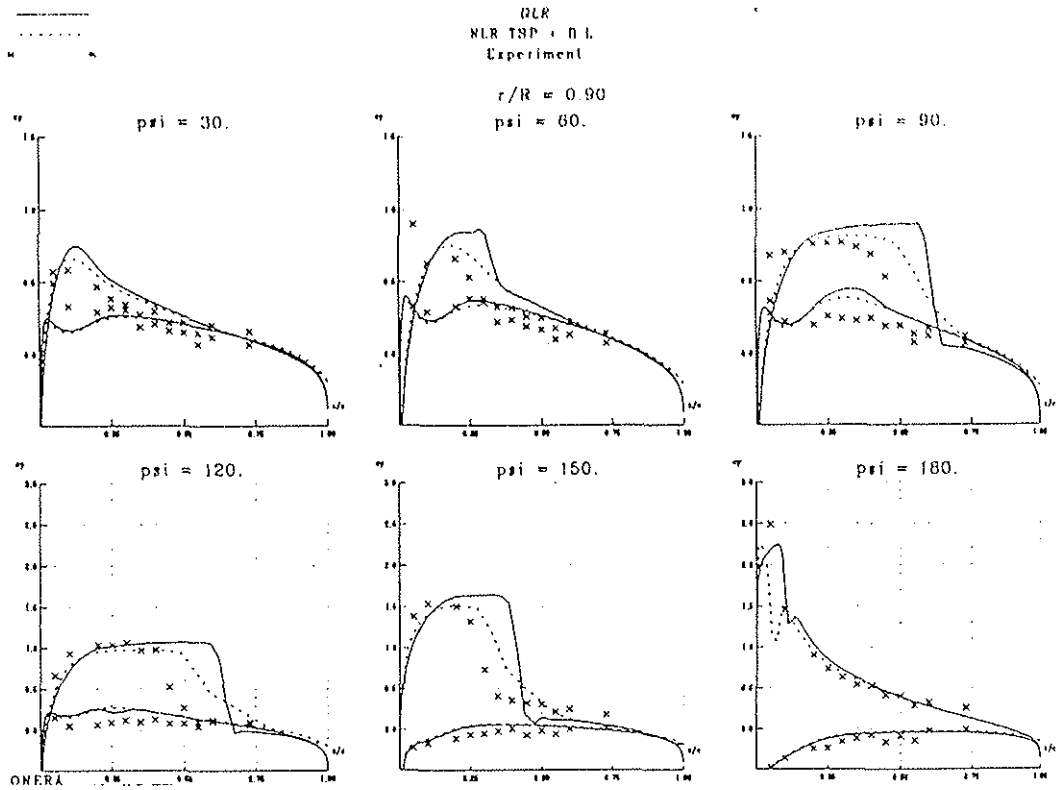

Fig. 8 - Lifting forward flight
$\mu = 0.43,\ M_{\omega R} = 0.63,\ C_L/\sigma = 0.066.$

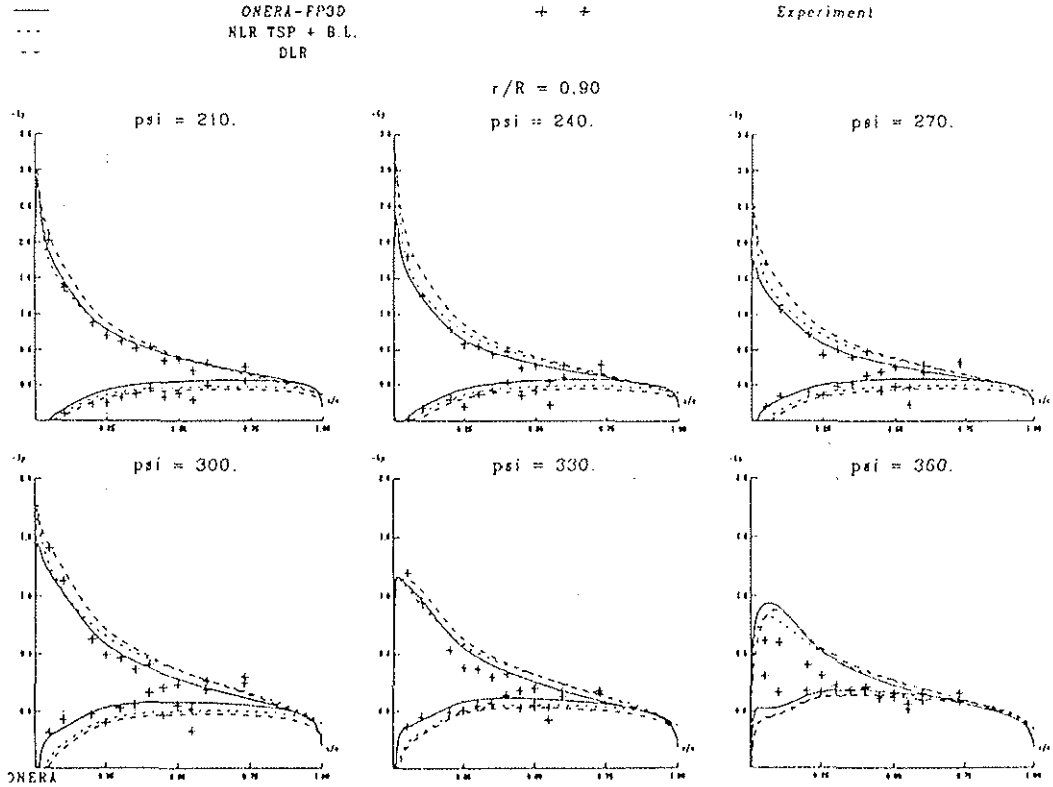

Fig. 9 - Lifting forward flight
$\mu = 0.43,\ M_{\omega R} = 0.63,\ C_L/\sigma = 0.066.$

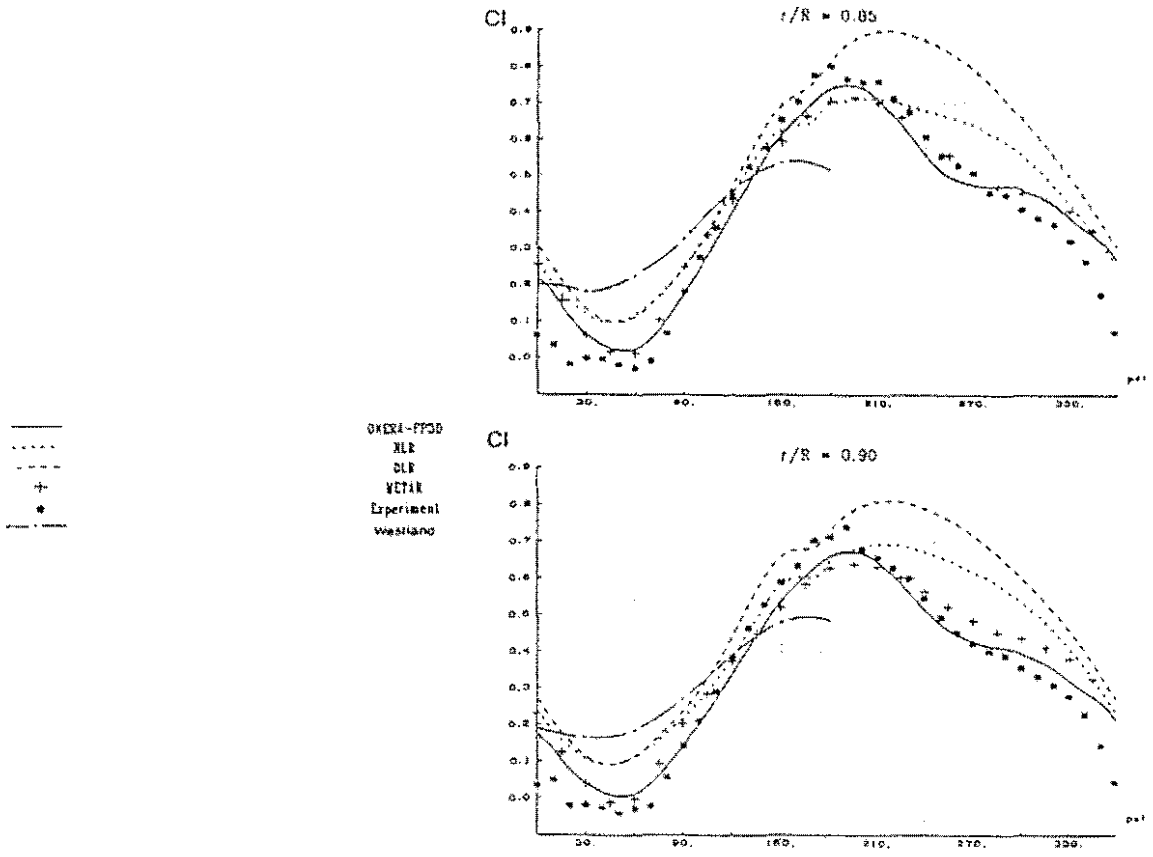

Fig. 10 - Lifting forward flight
$\mu = 0.43$, $M_{\omega R} = 0.63$, $C_L/\sigma = 0.066$.

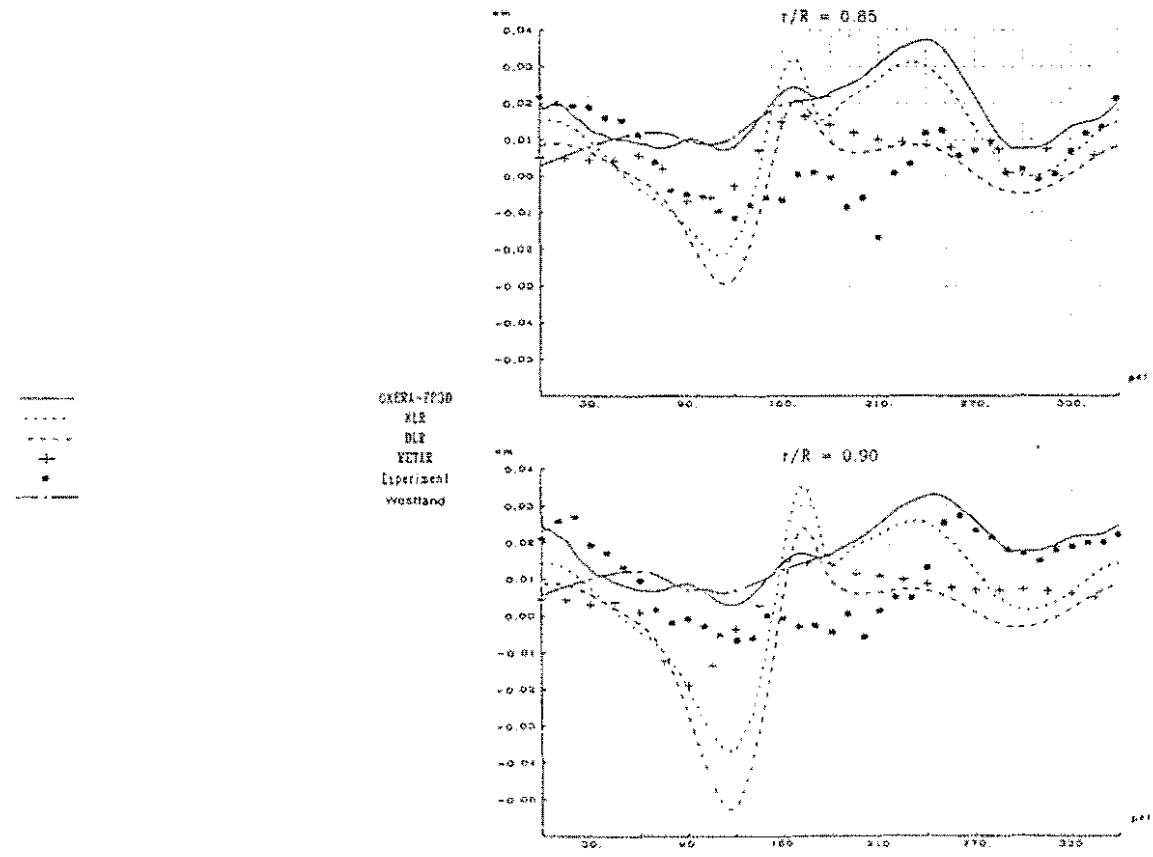

Fig. 11 - Lifting forward flight
$\mu = 0.43$, $M_{\omega R} = 0.63$, $C_L/\sigma = 0.066$.